

# Effect of position and volume of space-occupying liver lesions on liver function index in $^{99m}\text{Tc}$ -GSA scintigraphy

Ryotaro Tokorodani<sup>1</sup>, Hiromitsu Daisaki<sup>2</sup> , Yukinori Okada<sup>3</sup>, Eisuke Yasuda<sup>1</sup>

<sup>1</sup>Departments of Radiological Technology, Graduate School of Health Science, Suzuka University of Medical Science, Suzuka, Japan

<sup>2</sup>Departments of Gunma Prefectural College of Health Sciences, Maebashi, Japan

<sup>3</sup>Department of Radiology, Kochi Medical School Hospital, Kochi, Japan

[Received 29 VI 2020; Accepted 13 X 2020]

## Abstract

**Background:** The authors aimed to elucidate the effect of liver space-occupying lesions (SOL) on the quantitative index of the hepatic reserve, calculated using the dynamic planar image (LHLplanar), and a three-dimensional quantitative index (LHLSPECT) calculated using quantitative combined modality single-photon emission computed tomography (SPECT/CT).

**Material and Methods:** Water balloons of different volumes that simulated liver SOL were placed in various positions in the combined cardiac-liver phantom to examine the effects of liver SOL on visualization and quantitative indicators (LHLplanar and LHLSPECT). A 200 mL water balloon was placed in the anterior right, posterior right, left medial and left lateral lobes in the liver phantom to compare LHLplanar and LHLSPECT values with and without liver SOL at each position. Subsequently, volumes of those in the front of the right lobe were changed to 50 mL, 100 mL, 200 mL, and 400 mL, followed by statistically comparing LHLplanar and LHLSPECT values in the presence and absence of liver SOL.

**Results:** Despite the variation in the degree of defect accumulation with the location of the balloon when using frontal planar imaging, quantitative SPECT/CT imaging identified all defects. Multiple comparison analysis revealed that unlike LHLSPECT, the LHLplanar values changed according to liver SOL position and volume.

**Conclusions:** Liver SOL position and volume may affect the hepatic reserve assessments performed using LHLplanar values. In contrast, LHLSPECT is calculated using quantitative SPECT/CT and considers the effects of scattering and attenuation corrections. Therefore, LHLSPECT is a more accurate quantitative indicator of hepatic reserve than LHLplanar and is expected to facilitate future clinical research.

**KEY words:** galactosyl human serum albumin; LHL15; SPECT-CT; Liver SOL

Nucl Med Rev 2021; 24, 1: 1–10

## Introduction

It is imperative to preserve liver function during hepatectomies, the indication of which is determined via the preoperative assessment of hepatic reserve [1–3].  $^{99m}\text{Tc}$ -galactosyl human serum albumin ( $^{99m}\text{Tc}$ -GSA) specifically accumulates in the asialoglycoprotein receptor and is typically used to evaluate hepatic functional reserve [4–7]. Several analytical methods have currently been reported to evaluate hepatic functional reserve using preoperative  $^{99m}\text{Tc}$ -GSA receptor scintigraphy [8–11]. However, two of the most commonly

used indices that are easy to calculate and less device-dependent are LHL15 and HH15. The former can be calculated as a count ratio  $[L15/(H15+L15)]$  of the liver activity (L) to the heart activity  $[H] + \text{liver activity } [L]$  at 15 minutes after injection, while the latter can be calculated as a count ratio  $(H15/H3)$  of the heart activity (H) at 15 minutes (H15) to that at 3 minutes (H3) after injection. Typically, these indices are calculated using only the frontal planar images, which are acquired by using a gamma camera. However, the application of attenuation and scatter correction is difficult, considering the lack of depth or anatomical information in a frontal planar image. Also, a dynamic planar image cannot get enough counts due to time constraints. Therefore, scatter correction is not generally used in the dynamic planar image because it can cause increased statistical errors due to decreased counts. Additionally, it may demonstrate poorer accuracy in assessing liver functional reserve, because counts emitted from the liver are attenuated or scattered by the liver space-occupying lesions (SOLs). Moreover,

Correspondence to: Ryotaro Tokorodani  
 Department of Radiology,  
 Kochi Medical School Hospital, Kochi, Japan  
 185-1 Kohasu, Oko-cho, Nankoku-shi, Kochi, Japan  
 phone: +81-88-866-5811; fax: 088-886-2260  
 e-mail: jm-ryotaro\_tokorodani@kochi-u.ac.jp

the degree of the effect of attenuation depends on the location of the liver SOL [12, 13].

It has been reported that the diagnostic ability to occupy lesions can be improved by using SPECT [14, 15]. Furthermore, recent studies have reported that attenuation and scatter can be accurately corrected by using a correction algorithm for single-photon emission computed tomography in combination with computed tomography (SPECT/CT) [16–18]. In addition, Hasegawa et al. [19] reported a method to calculate an accurate index ( $LHL_{SPECT}$ ) of liver function reserve, which includes information about the reserve by using an attenuation and scatter corrected SPECT image for  $^{99m}\text{Tc}$ -GSA receptor scintigraphy. However, there have been no reports on the clinical accuracy concerning the influence of liver SOL on the liver function reserve evaluation via  $LHL_{SPECT}$ .

We aimed to elucidate the effect of liver SOLs on the  $LHL_{SPECT}$ -based index of the liver functional reserve and to evaluate and compare the usefulness of SPECT-CT imaging with planar imaging.

## Material and methods

### Equipment and acquisition conditions

The unique phantom configuration, which included the heart and the liver, was devised to simulate a human model of  $^{99m}\text{Tc}$ -GSA

distribution. First, the phantom heart was constructed by combining the cardiac phantom (model: RH-2, Kyoto Science Co., Ltd, Kyoto, Japan) and the outer cylinder of the National Electrical Manufacturers Association (NEMA) body phantom (Data Spectrum Co., Ltd. North Carolina, USA). Fixing components made with a three-dimensional (3D) printer were used to fix the phantom heart to the outer cylinder of the NEMA body phantom. Therefore, the position of the heart did not change across multiple acquisitions. Furthermore, two bubble wraps that simulated the lung field approximately -980 Hounsfield Unit were inserted and fixed on both sides of the phantom heart within the NEMA body phantom. A plastic tube of diameter 3 cm injected with dipotassium hydrogen phosphate was used to simulate the spine and was subsequently fixed with an adhesive tape [20]. Finally, the inside of the outer cylinder was filled with water. Figure 1 shows the components of the cardiac phantom and the appearance after assembly.

The outer cylinder of Flanged Jaszczak ECT Phantom ((Data Spectrum Co., Ltd. North Carolina, USA) was used for the trunk of the phantom liver. The liver portion of the liver/renal phantom (model: LKS, Kyoto Science Co., Ltd.) was fixed to the outer cylinder using a fixing component made with a 3D printer. Similar to the phantom heart, a plastic tube of 3 cm diameter injected with dipotassium hydrogen phosphate was placed on the dorsal side of the trunk and

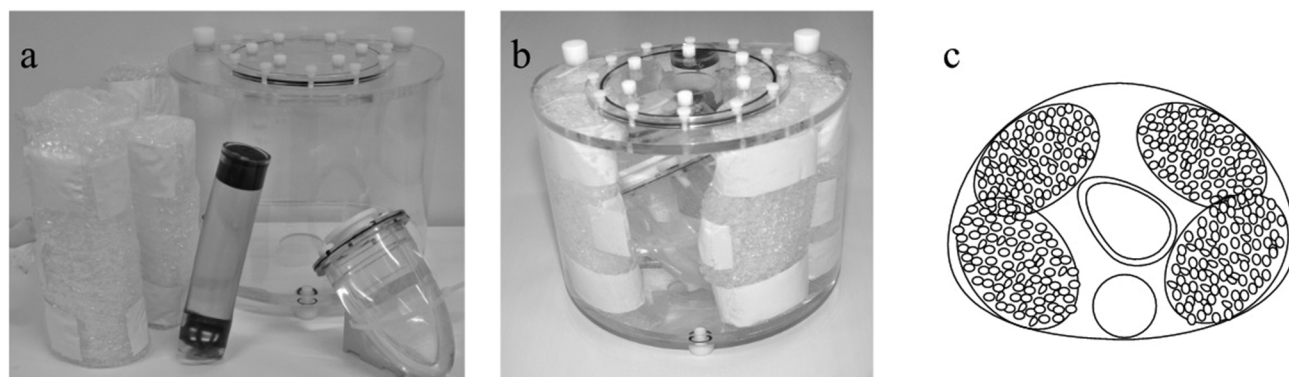


**Figure 1.** Appearance of cardiac phantom before (a) and after (b) assembly (c) schemas layout

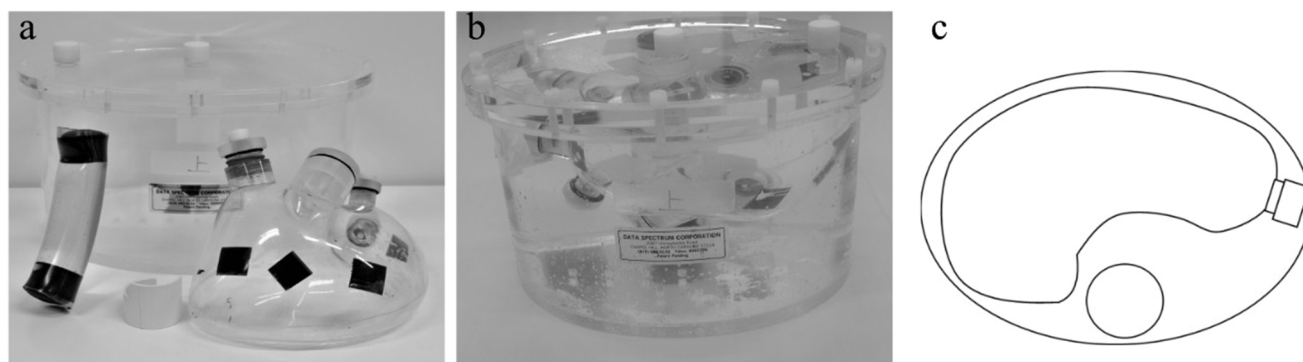


**Figure 2.** Appearance of liver phantom before (a) and after (b) assembly (c) schemas layout

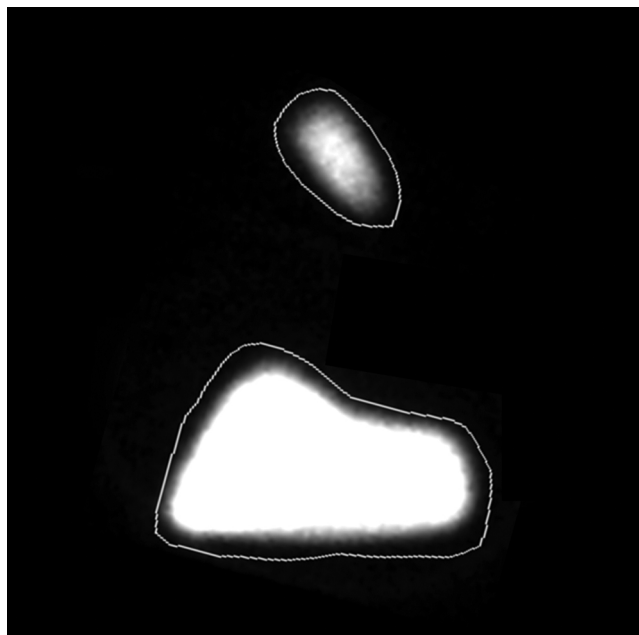


**Figure 3.** Regions of interest (ROI) setting in liver phantom

fixed with an adhesive tape. Figure 2 shows the components of the phantom liver and the appearance after assembly.

A  $^{99m}\text{Tc}$  solution of 100 kBq/mL corresponding to the clinical liver radioactivity concentration was filled in the liver phantom (1600 mL) based on the study by Toritsuka et al. [21] as the reference for All data acquisition. Since the normal value of LHL15 is approximately 0.900, the cardiac phantom (133 mL) was filled with 16.0 MBq of  $^{99m}\text{Tc}$  solution, and the theoretical value of LHL15 was adjusted to 0.909.

All data acquisition was performed using a SPECT/CT scanner named Symbia T6 (Siemens Healthcare Co., Ltd, Munich, Germany) equipped with a low-energy high-resolution collimator Hole length 24.1 mm, Septal thickness 0.16 mm, Hole diameter across the flats 1.11 mm. Data acquisition in planar imaging was performed using parameters of matrix size  $128 \times 128$ , zoom

1.0, and pixel size 4.8 mm. Dynamic planar imaging was performed for 18 minutes at 10 seconds/frame  $\times$  108 frames under conditions identical to the authors' clinical protocol. Following this, SPECT imaging was performed at  $128 \times 128$  matrix, zoom 1.0, pixel size 4.8 mm, 360-degree acquisition (60 directions, 6-degree steps), and 12 seconds/step. Even though scatter correction was not performed in the dynamic planar imaging, the triple energy window (TEW) method was used for the same in SPECT imaging. In this method, the main window was set at  $140 \text{ keV} \pm 10\%$ , along with a 7% energy width of two sub-windows located on both sides of the main window. CT-based attenuation correction method was used for attenuation correction. Furthermore, CT scanning was performed at 130 kV for the tube voltage, Quality Reference was set at 120 mA with auto exposure control for the tube current, 1.0 s/rot for the scan time, and 4 mm for the image slice thickness. Image reconstruction and count analysis were performed using the Syngo MI Apps version VA60C (Siemens Healthcare Co., Ltd, Munich, Germany). The SPECT images were reconstructed using a 3D ordered subset expectation-maximization algorithm with collimator aperture correction called Flash-3D. The SPECT image reconstruction parameters of Flash-3D were set to 10 subsets and 6 iterations, and then image filtering for noise reduction was performed using a 3D Gaussian post-filtering function with 9.6 mm full width at half maximum.

#### Calculation of $LHL_{\text{planar}}$ and $LHL_{\text{SPECT}}$

$LHL_{\text{planar}}$  was calculated using regional counts of planar imaging of the heart ( $H_{\text{planar}}$ ) and liver ( $L_{\text{planar}}$ ) at 15 minutes, as follows:

$$LHL_{\text{planar}} = L_{\text{planar}} / (L_{\text{planar}} + H_{\text{planar}}) \quad (1)$$

Here,  $L_{\text{planar}}$  and  $H_{\text{planar}}$  were obtained by regions of interest (ROI) that were manually drawn on both the liver and the heart, respectively, on the two-dimensional planar image. All measurements were performed by three radiological technologists). Figure 3 shows an example of the ROI placed on the planar image.

$LHL_{\text{SPECT}}$  was calculated using regional counts of SPECT-CT imaging of the heart ( $H_{\text{SPECT}}$ ) and liver ( $L_{\text{SPECT}}$ ) as follows:

$$LHL_{\text{SPECT}} = L_{\text{SPECT}} / (L_{\text{SPECT}} + H_{\text{SPECT}}) \quad (2)$$

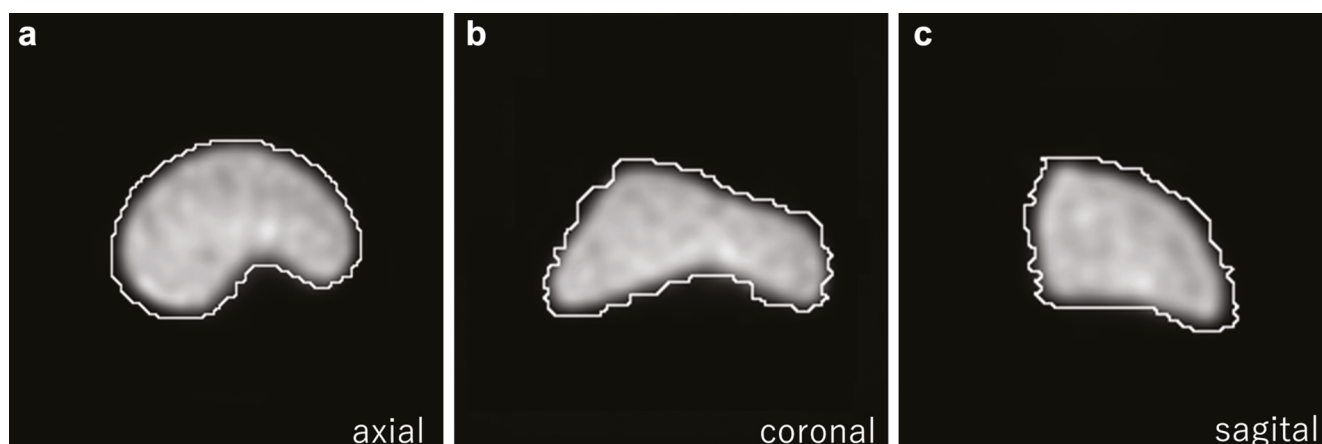


**Figure 4.** Volume of interest (VOI) setting at the center slice of the liver phantom

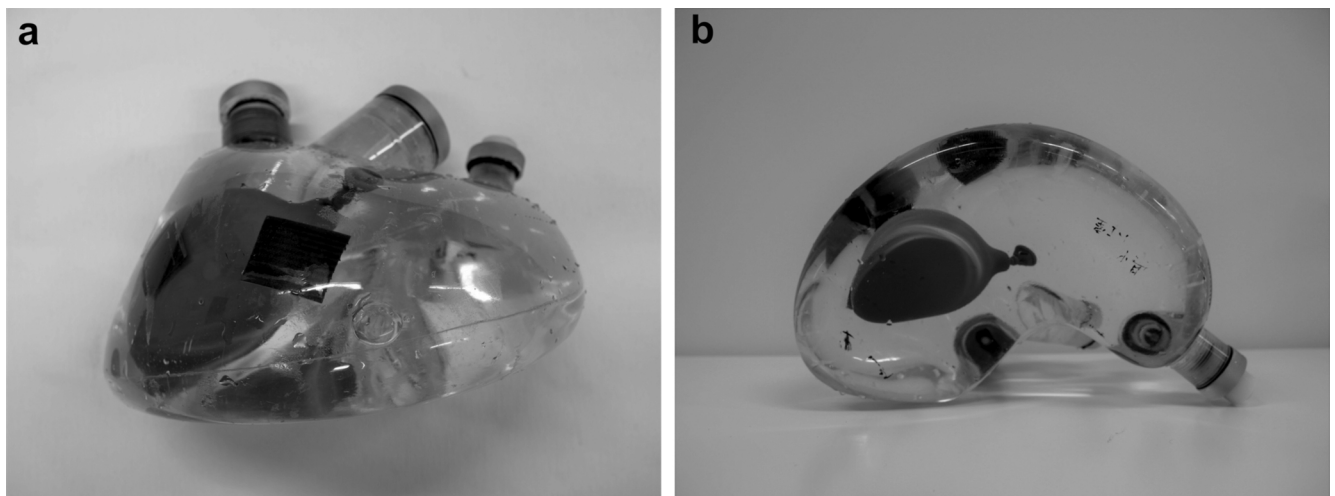


**Figure 5.** Liver phantom with water balloons

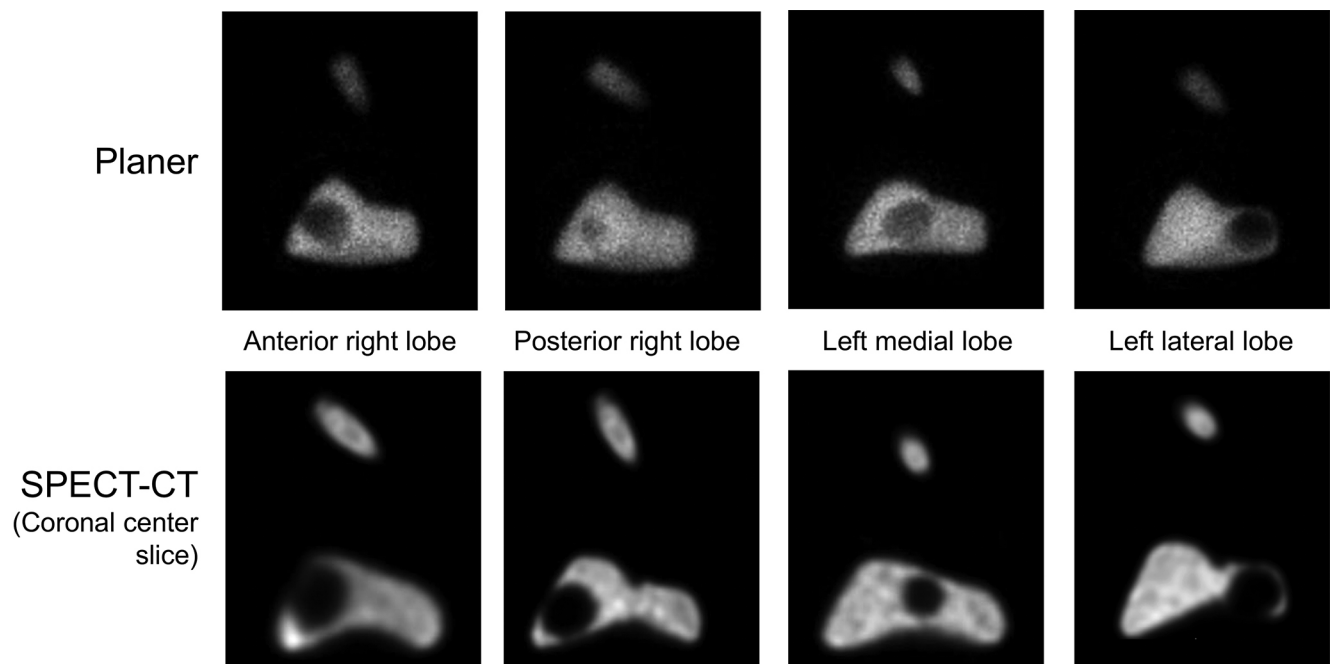


**Figure 6.** planar imaging (a) and SPECT-CT imaging (b) obtained using phantoms with liver space-occupying lesion (SOL) placed at different positions

Here,  $L_{\text{SPECT}}$  and  $H_{\text{SPECT}}$  are obtained by volume of interest (VOI) that was manually drawn on both the liver and the heart, respectively, on the SPECT-CT image. Both  $LHL_{\text{planar}}$  and  $LHL_{\text{SPECT}}$  were measured 10 times by three radiological technologists, following which each median value was calculated. Figure. 4 shows an example of the VOI placed on the SPECT-CT image.

### **Evaluation of position dependency**

A balloon containing 200 mL of water simulating liver SOL was placed at different positions in the anterior right, posterior right, left medial and left lateral lobes in the liver phantom to change the distribution of radioactivity within the liver. When the water balloon

was inserted, a certain amount of water was withdrawn from the liver phantom and the theoretical value of LHL15 was always adjusted to 0.909 by injecting 160 MBq of  $^{99m}\text{Tc}$  solution. The water balloon was secured to the liver phantom using a hook and loop fastener to ensure repeatability. Figure 5 shows the appearance of a liver phantom with a secured water balloon.

After changing the position of the water balloon, both frontal planar and SPECT-CT imaging were performed, and LHL15 calculated using each imaging method was compared. Bland-Altman plots were constructed to assess measurement agreement between equivalent measurements [22]. When the confidence interval does not include 0, it is determined that there is a fixed error if the

**Table 1.**  $LHL_{planar}$  and  $LHL_{SPECT}$  calculated by phantom with space occupying lesions of liver located in different positions

| Water balloon position | None     | Posterior right lobe | Anterior right lobe | Left medial lobe | Left lateral lobe |
|------------------------|----------|----------------------|---------------------|------------------|-------------------|
| $LHL_{planar}$         | 0.911    | 0.909                | 0.902               | 0.907            | 0.909             |
| Heart counts           | 822233   | 814951               | 811176              | 813525           | 81286             |
| Liver counts           | 8411452  | 8150716              | 7428690             | 7918294          | 8151403           |
| $LHL_{SPECT}$          | 0.912    | 0.911                | 0.911               | 0.911            | 0.911             |
| Heart counts           | 1311653  | 1304817              | 1299157             | 1288636          | 1335552           |
| Liver counts           | 13567975 | 13401944             | 13231695            | 13292786         | 13668551          |

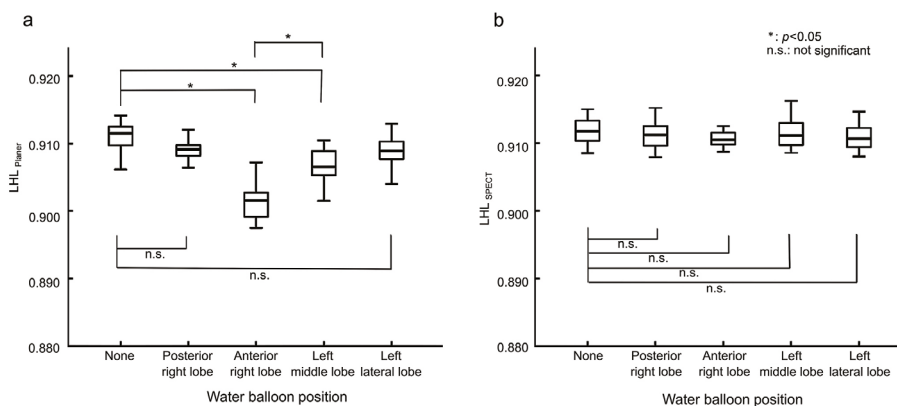


**Figure 7.** Effect of liver space-occupying lesion (SOL) position on  $LHL_{planar}$  (a) and  $LHL_{SPECT}$  (b)

measured value exists in either the positive direction or the negative direction. The software used to create the Bland-Altman plot was Microsoft Excel version 2016 (Microsoft Corporation Co., Ltd, Redmond, State of Washington).

**Evaluation of volume dependency**

The water balloon was fixed at the front of the right lobe and its volume was changed to 50, 100, 200 and 400 mL. Planar imaging and SPECT-CT imaging were performed for each volume. Bland-Altman plots were constructed to assess measurement agreement between equivalent measurements.

**Statistical Analysis**

$LHL_{planar}$  and  $LHL_{SPECT}$  values with the water balloon placed at each position in the liver phantom were independently compared with those without SOLs as the standard reference. The Kruskal-Wallis test was used for the comparison, and the Mann-Whitney U test was performed for the multiple comparison test, which was corrected using the Bonferroni method. The significance level was set at  $p < 0.05$ . Statistical analysis software used was EZR version 1.37 (Jichi Medical School Saitama Medical Center, Saitama, Japan) [23].

**Results**

**Position dependency evaluation**

Figure.6 shows the images obtained with each imaging technique, changing the position of the water balloon.

Changes in the degree of defect accumulation associated with the location of the balloon are depicted via frontal planar imaging

(Fig. 6a). A visual assessment revealed that defects were clearly visible when the water balloons were placed in the right upper, left medial, and left lateral lobes, even though the defect was only identified as a low accumulation region in cases where the water balloon was placed in the posterior right lobe. However, since both attenuation and scatter correction were applied to SPECT-CT imaging, it was able to clearly identify all defects regardless of the position of the water balloon.

Table 1 shows the average of total ROI counts of the heart and the liver,  $LHL_{planar}$  and  $LHL_{SPECT}$  for each water balloon position.

The position dependency effect of each LHL15 is shown by a box and whisker plot in Figure 7.

The median  $LHL_{planar}$  values calculated by planar imaging were: 0.911, 0.909, 0.902, 0.906, and 0.909 in the absence of a water balloon, water balloon at the anterior right lobe, posterior right lobe, left medial lobe, and left lateral lobe, respectively. The Kruskal-Wallis test demonstrated a significant difference ( $p < 0.001$ ), and  $LHL_{planar}$  showed a significant difference in the anterior right lobe ( $p < 0.001$ ) and the left medial lobe ( $p = 0.012$ ) compared to without water balloon. Additionally, the anterior right lobe showed a significant difference compared to the left medial lobe ( $p < 0.001$ ). However, no significant difference in the posterior right lobe ( $p = 0.262$ ) and the left lateral lobe ( $p = 0.618$ ) was observed.

The median values of  $LHL_{SPECT}$  calculated by SPECT/CT imaging were: 0.912, 0.911, 0.910, 0.911, and 0.911 in the absence of a water balloon, water balloon at the anterior right lobe, the posterior right lobe, the left medial lobe, and the left lateral lobe, respectively. There was no significant difference according to the Kruskal-Wallis test ( $p = 0.266$ ).

**Table 2.**  $LHL_{planar}$  and  $LHL_{SPECT}$  calculated by phantom with different volume of space occupying lesions of liver

| Water balloon volume | None     | 50 mL    | 100 mL   | 200 mL   | 400 mL   |
|----------------------|----------|----------|----------|----------|----------|
| $LHL_{planar}$       | 0.911    | 0.912    | 0.910    | 0.901    | 0.891    |
| Heart counts         | 822233   | 819828   | 834696   | 810514   | 819583   |
| Liver counts         | 8411452  | 8511024  | 8462878  | 7411870  | 6725406  |
| $LHL_{SPECT}$        | 0.912    | 0.911    | 0.910    | 0.911    | 0.911    |
| Heart counts         | 1311653  | 1361975  | 1389435  | 1340746  | 1342052  |
| Liver counts         | 13567975 | 13950857 | 14072066 | 13658601 | 13670859 |

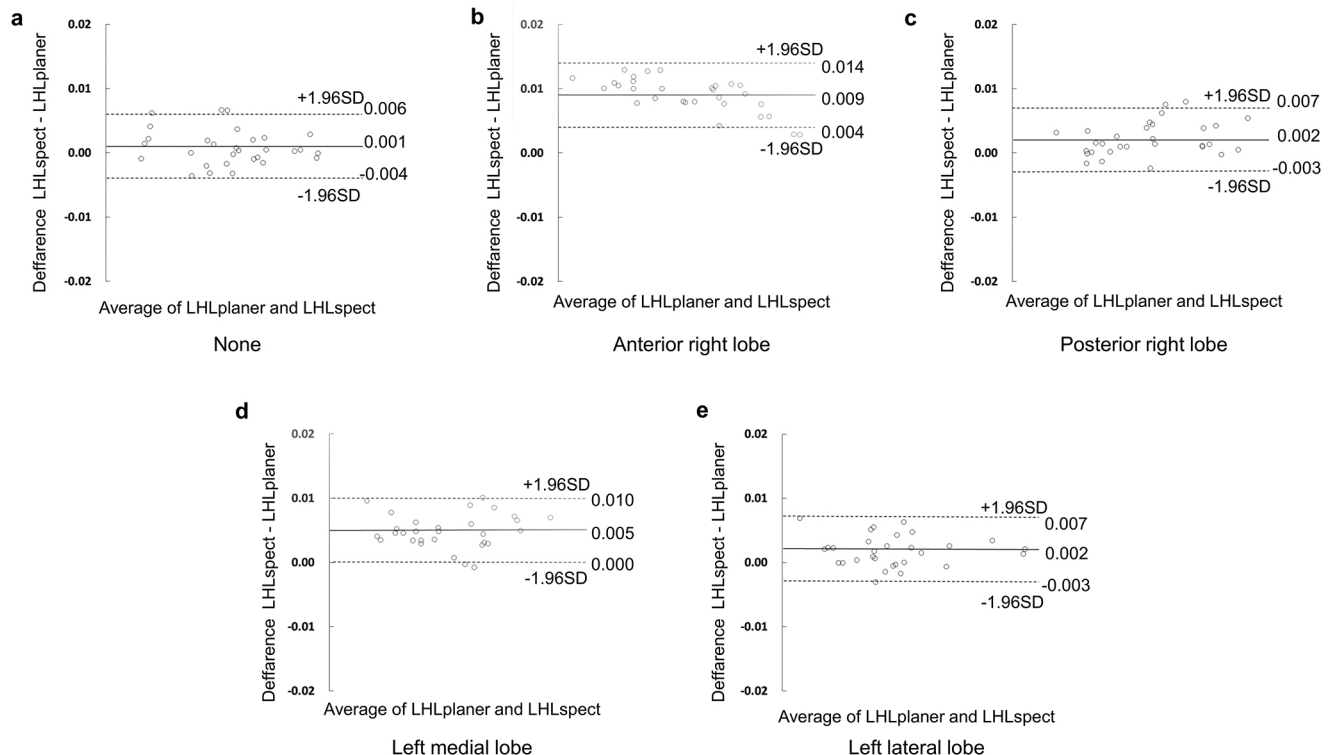
**Figure 8.** Bland-Altman plots for regions of interest (ROI) comparisons from  $LHL_{planar}$  and  $LHL_{SPECT}$  for each water balloon position

Figure 8 shows Bland-Altman plots for ROI comparisons from  $LHL_{planar}$  and  $LHL_{SPECT}$  for each water balloon position.

According to Bland-Altman analysis, there was a fixed bias in the anterior right lobe and left medial lobe.

### Volume dependency evaluation

Figure 9 shows the images obtained by each imaging method with different water balloon volumes.

In the planar phantom images, the degree of defect changed according to the changes in the water balloon volumes, whereas the degree of the defect was equivalent in the SPECT/CT phantom images, and the area was accurately depicted. Furthermore, SPECT/CT imaging was able to depict the liver uniformly.

Table 2 shows the average of total ROI counts of the heart and liver,  $LHL_{planar}$  and  $LHL_{SPECT}$  for each water balloon volume.

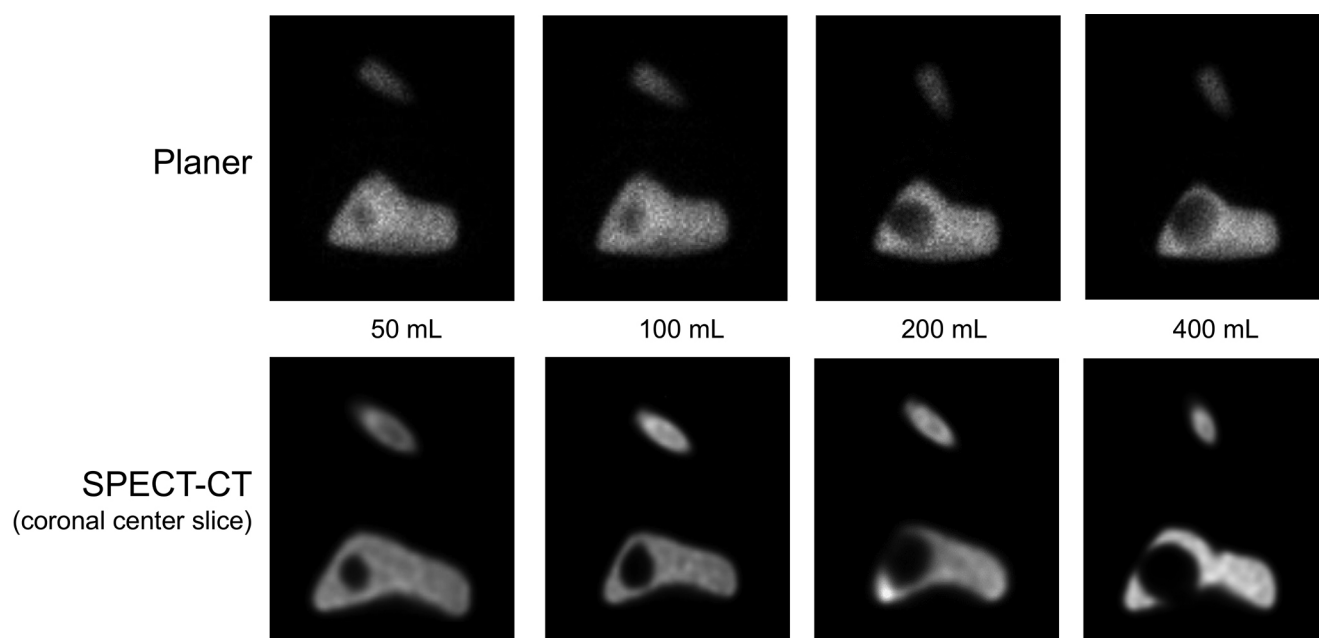
The volume dependency effect of each LHL15 is shown by a box and whisker plot in Figure 10.

Median LHL plane values calculated by frontal planar imaging were 0.911 in the absence of a water balloon and 0.912, 0.910, 0.901 and 0.892 for 50, 100, 200 and 400 mL water balloons, respectively. The Kruskal-Wallis test showed a significant difference ( $p < 0.001$ ), and  $LHL_{planar}$  showed a significant difference in 200 mL ( $p < 0.001$ ) and 400 mL ( $p < 0.001$ ) water balloons compared with the one without the water balloon. However, no significant difference was found with the 50 mL ( $p = 1.000$ ) and 100 mL ( $p = 1.000$ ) water balloons.

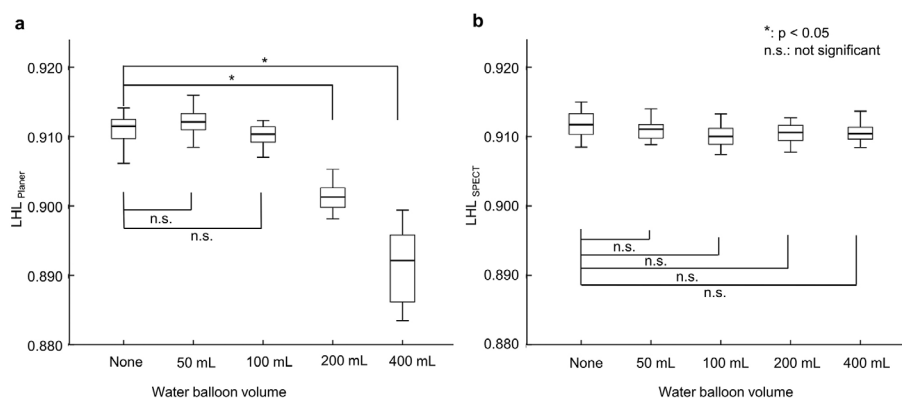
In contrast, median  $LHL_{SPECT}$  values obtained with SPECT-CT imaging were 0.912 without the water balloon and 0.911, 0.910, 0.911 and 0.910 for the 50, 100, 200 and 400 mL water balloons, respectively. The Kruskal-Wallis test showed no significant difference ( $p = 0.157$ ).

Figure 11 shows Bland-Altman plots for ROI comparisons from  $LHL_{planar}$  and  $LHL_{SPECT}$  for different water balloon volumes.

According to Bland-Altman analysis, there was a fixed bias in the 200 mL and 400 mL water balloons.



**Figure 9.** planar imaging (a) and SPECT-CT imaging (b) obtained using phantoms with liver space-occupying lesion (SOL) with different volumes



**Figure 10.** Effect of liver space-occupying lesion (SOL) volume on  $\text{LHL}_{\text{planar}}$  (a) and  $\text{LHL}_{\text{SPECT}}$  (b)

## Discussion

$^{99m}\text{Tc}$ -GSA specifically accumulates in asialoglycoprotein receptors on the surface of hepatocytes, and the accumulation reflects liver function. It is also known that  $^{99m}\text{Tc}$ -GSA does not accumulate in tumours without the asialoglycoprotein receptor or in highly fibrotic hepatocytes. The hepatic clearance of  $^{99m}\text{Tc}$ -GSA receptor scintigraphy performed preoperatively has been reported as a useful index to predict postoperative liver function [7]. Several centres currently evaluate hepatic reserve by  $\text{LHL}_{\text{planar}}$  imaging. However, hepatic reserve assessment using the frontal planar image cannot take depth or anatomical information into account. Furthermore, the position and volume of the liver SOL influence the result of the assessment. In this study, the authors evaluated the effect of the position and volume of liver SOL on  $\text{LHL}_{\text{planar}}$  and examined how these effects were improved by SPECT-CT imaging with various corrections.

In the position dependency evaluation using the frontal planar image, the water balloon was visualized as a defect when it was present in the right anterior lobe in the liver phantom. However, the visibility of the defect changed with a change in the position of the water balloon. This suggests that it is not possible to detect the counts from the normal liver present behind the liver SOL (simulated with a water balloon) causing attenuation or scattering at the frontal detector. This is also apparent from the fact that  $\text{LHL}_{\text{planar}}$  showed no significant decrease from the theoretical value of 0.909 when the water balloon was placed in the right anterior and left medial lobe, whereas  $\text{LHL}_{\text{planar}}$  was significantly reduced when the water balloon was placed in the right posterior and left lateral lobes. Furthermore,  $\text{LHL}_{\text{planar}}$  decreased when the balloon was placed in the right anterior rather than left medial lobe, suggesting that a larger normal liver volume in the presence of a liver SOL was associated with a greater possibility of attenuation or scattering. Similarly, in the Bland-Altman

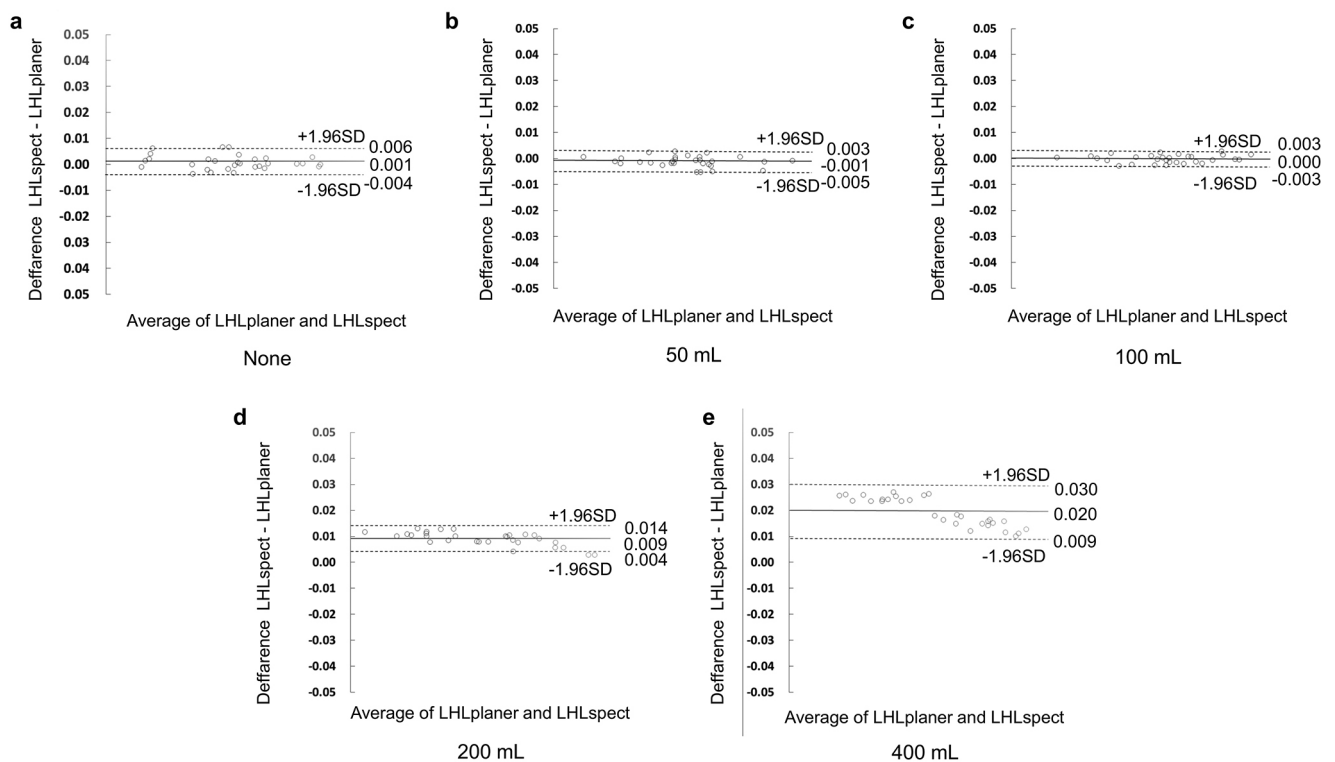


**Figure 11.** Bland-Altman plots for regions of interest (ROI) comparisons from  $LHL_{planar}$  and  $LHL_{SPECT}$  for different water balloon volumes

analysis, was observed a fixed bias only in the right posterior and left lateral lobes.

Alternatively, in the phantom images obtained by SPECT/CT imaging, all of the liver and defect parts were correctly imaged by a certain degree of correction, regardless of the attenuation or scattering associated with the position of the water balloon. Additionally,  $LHL_{SPECT}$  demonstrated nearly theoretical values regardless of the attenuation or scattering associated with the position of the water balloon. Furthermore, there was no statistically significant difference among different water balloon positions. This could be attributed to the fact that position dependency was eliminated by imaging from 360 degrees and photon attenuation or scatter caused by the water balloon placed within the liver region was corrected by attenuation correction using CT images and scatter correction. Additionally, since the liver is located to the right of the trunk, the resolution recovery effect may have contributed to the improvement of dependency.

considering the evaluation of volume dependency, the phantom images obtained by frontal planar imaging demonstrated an increase in the defect area with an increase in the water balloon volume. Similarly, Bland-Altman analysis reported the presence of a fixed bias only in 200 mL and 400 mL water balloons. This implied an increase in the uncounted area of normal hepatocytes present behind the liver SOL, suggesting that the attenuation or scattering effect was volume dependent. However, the phantom image obtained through SPECT/CT imaging was able to correctly image both the liver and the defect region as in the position-dependent evaluation regardless of the volume of a water balloon, and  $LHL_{SPECT}$  reported nearly the same outcomes as the theoretical value. This result revealed that the effects of attenuation and scattering

were accurately corrected by the CT attenuation correction and scatter correction method (TEW method) applied by the SPECT-CT scanner used in this study.

$LHL_{planar}$  with dynamic planar imaging has been widely used to assess hepatic reserve. However, this study suggests that in the case of hepatic reserve evaluation using only planar imaging, the measurement results changed depending on the position and volume of the liver SOL. This may be a technical limitation of accurate clinical evaluation of hepatic reserve using planar imaging. However,  $LHL_{SPECT}$  values that were calculated using SPECT/CT imaging in this study were not affected by the position and volume of liver SOL, suggesting that SPECT/CT imaging is preferable to  $^{99m}Tc$ -GSA receptor scintigraphy to assess hepatic reserve. Considering this approach can further improve the clinical significance of SPECT/CT imaging in indexing the liver functional reserve. A statistically significant decrease in  $LHL_{15}$  may affect the indications for surgery in patients with decreased liver function. In the future, high-precision indicators calculated by SPECT/CT should be considered as a method to replace or compensate traditional planar imaging methods with position and volume dependency as elucidated by the presented study. However, dynamic imaging using SPECT/CT was inferior to dynamic imaging via a frontal planar image in time resolution. Furthermore, it is imperative to carefully monitor the patient to ensure safety during the examination because the detector rotates multiple times around the patient when using dynamic SPECT/CT imaging.

This study is only a phantom experiment and does not consider actual pharmacokinetics. The first limitation of this study is the  $LHL_{planar}$  reported in this study may be different from the existing indicators (e.g.  $LHL_{15}$ ) used in clinical practice. Further

studies comparing the two approaches using clinical data would be required. SPECT-CT has reportedly been considered an indicator of regional accumulation in the liver [8, 24–25]. Although these studies used SPECT alone, which may include position and volume dependencies, it is possible to reduce these dependencies by using SPECT-CT imaging similar to this study. The second limitation of this study is the position and size of the water balloon in the right lobe. The phantom volume was not large enough to precisely move the water balloon, contrary to what is observed in actual clinical practice, SOL may exist in the middle of the right lobe. Also, in clinical practice, the effect of SOL size depends on liver activity. The third limitation is the calculation method of LHL15. LHL15 is usually calculated using only the frontal planar images, but additional views from the posterior planar images may improve the position- and volume-dependent dependence and should be considered.

## Conclusions

Accuracy of the quantitative indicator was limited because  $LHL_{\text{planar}}$ , which is an index to evaluate hepatic functional reserve using planar imaging, demonstrated position and volume-based dependencies due to the presence of liver SOL. However,  $LHL_{\text{SPECT}}$  obtained by SPECT-CT imaging with some corrections did not show the position or volume dependencies by liver SOL, highlighting the high degree of accuracy of  $LHL_{\text{SPECT}}$  as a quantitative indicator to assess hepatic functional reserve in clinical practice.

## Conflict of interest

Author Hiromitsu Daisaki has received research grants from Nihon Medi-Physics Co., Ltd.

## Human and animal rights

This article does not contain any studies performed with human participants and animals.

## Informed consent

Informed consent for this study was not required because it involved no research involving human participants.

## References

- Farges O, Malassagne B, Flejou JF, et al. Risk of major liver resection in patients with underlying chronic liver disease: a reappraisal. *Ann Surg.* 1999; 229(2): 210–215, doi: [10.1097/00000658-199902000-00008](https://doi.org/10.1097/00000658-199902000-00008), indexed in Pubmed: [10024102](https://pubmed.ncbi.nlm.nih.gov/10024102/).
- Nagasue N, Kohno H, Chang YC, et al. Liver resection for hepatocellular carcinoma. Results of 229 consecutive patients during 11 years. *Ann Surg.* 1993; 217(4): 375–384, doi: [10.1097/00000658-199304000-00009](https://doi.org/10.1097/00000658-199304000-00009), indexed in Pubmed: [8385442](https://pubmed.ncbi.nlm.nih.gov/8385442/).
- Scheele J, Stangl R, Altendorf-Hofmann A, et al. Indicators of prognosis after hepatic resection for colorectal secondaries. *Surgery.* 1991; 110(1): 13–29, indexed in Pubmed: [1866690](https://pubmed.ncbi.nlm.nih.gov/1866690/).
- Morell AG, Gregoriadis G, Scheinberg IH, et al. The role of sialic acid in determining the survival of glycoproteins in the circulation. *J Biol Chem.* 1971; 246(5): 1461–1467, indexed in Pubmed: [5545089](https://pubmed.ncbi.nlm.nih.gov/5545089/).
- Orita Y, Onodera A, Natsume T. Devised a New Preoperative Simulation Using  $^{99m}\text{Tc}$ -GSA SPECT Quantitative Method for Liver Resection. *Japanese Journal of Radiological Technology.* 2016; 72(1): 50–57, doi: [10.6009/ijrt.2016\\_jsrt\\_72.1.50](https://doi.org/10.6009/ijrt.2016_jsrt_72.1.50).
- Okabe H, Beppu T, Hayashi H, et al. Rank classification based on the combination of indocyanine green retention rate at 15 min and (99m) Tc-DTPA-galactosyl human serum albumin scintigraphy predicts the safety of hepatic resection. *Nucl Med Commun.* 2014; 35(5): 478–483, doi: [10.1097/MNM.0000000000000075](https://doi.org/10.1097/MNM.0000000000000075), indexed in Pubmed: [24686196](https://pubmed.ncbi.nlm.nih.gov/24686196/).
- limuro Y, Kashiwagi T, Yamanaka J, et al. Preoperative estimation of asialoglycoprotein receptor expression in the remnant liver from CT/99mTc-GSA SPECT fusion images correlates well with postoperative liver function parameters. *J Hepatobiliary Pancreat Sci.* 2010; 17(5): 673–681, doi: [10.1007/s00534-010-0264-6](https://doi.org/10.1007/s00534-010-0264-6), indexed in Pubmed: [20703846](https://pubmed.ncbi.nlm.nih.gov/20703846/).
- Yoshida M, Shiraishi S, Sakaguchi F, et al. A quantitative index measured on 99mTc GSA SPECT/CT 3D fused images to evaluate severe fibrosis in patients with chronic liver disease. *Japanese Journal of Radiology.* 2012; 30(5): 435–441, doi: [10.1007/s11604-012-0072-9](https://doi.org/10.1007/s11604-012-0072-9).
- Shuke N, Okizaki A, Kino S, et al. Functional mapping of regional liver asialoglycoprotein receptor amount from single blood sample and SPECT. *J Nucl Med.* 2003; 44(3): 475–482, indexed in Pubmed: [12621017](https://pubmed.ncbi.nlm.nih.gov/12621017/).
- Kaibori M, Ha-Kawa SK, Ishizaki M, et al. HA/GSA-Rmax ratio as a predictor of postoperative liver failure. *World J Surg.* 2008; 32(11): 2410–2418, doi: [10.1007/s00268-008-9725-3](https://doi.org/10.1007/s00268-008-9725-3), indexed in Pubmed: [18758848](https://pubmed.ncbi.nlm.nih.gov/18758848/).
- Miki K, Kubota K, Kokudo N, et al. Asialoglycoprotein receptor and hepatic blood flow using technetium-99m-DTPA-galactosyl human serum albumin. *J Nucl Med.* 1997; 38(11): 1798–1807, indexed in Pubmed: [9374359](https://pubmed.ncbi.nlm.nih.gov/9374359/).
- Morikatsu Y, Toru B, Shinya S, et al. Noriko, 99mTc-GSA SPECT/CT fused images for assessment of hepatic function and hepatectomy planning. *Ann Transl Med.* 2015; 3: 17.
- Tokorodani R, Sumiyoshi T, Okabayashi T, et al. Liver fibrosis assessment using 99mTc-GSA SPECT/CT fusion imaging. *Jpn J Radiol.* 2019; 37(4): 315–320, doi: [10.1007/s11604-019-00810-w](https://doi.org/10.1007/s11604-019-00810-w), indexed in Pubmed: [30656542](https://pubmed.ncbi.nlm.nih.gov/30656542/).
- Matumoto T, Iinuma TA, Ishikawa T, et al. [SOL-detectability of liver SPECT-analysis of the structure of ROC-curve]. *Radioisotopes.* 1985; 34(9): 486–492, doi: [10.3769/radioisotopes.34.9\\_486](https://doi.org/10.3769/radioisotopes.34.9_486), indexed in Pubmed: [3878978](https://pubmed.ncbi.nlm.nih.gov/3878978/).
- Mori Y, Kawakami K, Machida K, et al. A cooperative group study of clinical efficacy of the liver SPECT. *Radioisotopes.* 1987; 36(9): 457–464, doi: [10.3769/radioisotopes.36.9\\_457](https://doi.org/10.3769/radioisotopes.36.9_457).
- Zeintl J, Vija AH, Yahil A, et al. Quantitative accuracy of clinical 99mTc SPECT/CT using ordered-subset expectation maximization with 3-dimensional resolution recovery, attenuation, and scatter correction. *J Nucl Med.* 2010; 51(6): 921–928, doi: [10.2967/jnumed.109.071571](https://doi.org/10.2967/jnumed.109.071571), indexed in Pubmed: [20484423](https://pubmed.ncbi.nlm.nih.gov/20484423/).
- Nakahara T, Daisaki H, Yamamoto Y, et al. Use of a digital phantom developed by QIBA for harmonizing SUVs obtained from the state-of-the-art SPECT/CT systems: a multicenter study. *EJNMMI Res.* 2017; 7(1): 53, doi: [10.1186/s13550-017-0300-5](https://doi.org/10.1186/s13550-017-0300-5), indexed in Pubmed: [28639254](https://pubmed.ncbi.nlm.nih.gov/28639254/).
- Tokorodani R, Ueta K, Kume T, et al. Evaluation of Normal Bone Standardized Uptake Values Using Quantitative SPECT with Improved Spatial Resolution. *Kakuigaku gijyutu.* 2017(3): 201–210.
- Hasegawa D, Onishi H. Evaluation of Accuracy for Quantitative Predictor of Hepatic Functional Reserve Using Planar and SPECT Images in the Tc-GSA Scintigraphy. *Nihon Hoshasen Gijyutsu Gakkai Zasshi.* 2017; 73(10): 1055–1060, doi: [10.6009/ijrt.2017\\_JSRT\\_73.10.1055](https://doi.org/10.6009/ijrt.2017_JSRT_73.10.1055), indexed in Pubmed: [29057777](https://pubmed.ncbi.nlm.nih.gov/29057777/).
- de Dr, Strijckmans V, Almeida P, et al. Boneequivalent liquid solution to asses accuracy of transmission measurements in SPECT and PET. *IEEE Trans Nucl Sci.* 1997; 44: 1186–90.
- Torizuka K, Ha-Kawa SK, Kudo M, et al. Phase III multi-center clinical study on 99mTc-GSA, a new agent for functional imaging of the liver. *Kaku Igaku.* 1992(29): 159–181.

22. Bland JM, Altman DG. Statistical methods for assessing agreement between two methods of clinical measurement. *Lancet*. 1986; 1(8476): 307–310, indexed in Pubmed: [2868172](#).
23. Kanda Y. Investigation of the freely available easy-to-use software 'EZ' for medical statistics. *Bone Marrow Transplant*. 2013; 48(3): 452–458, doi: [10.1038/bmt.2012.244](#), indexed in Pubmed: [23208313](#).
24. Imaeda T, Kanematsu M, Asada S, et al. Utility of Tc-99m GSA SPECT imaging in estimation of functional volume of liver segments in health and liver diseases. *Clin Nucl Med*. 1995; 20(4): 322–328, doi: [10.1097/00003072-199504000-00008](#), indexed in Pubmed: [7788989](#).
25. Kotani K, Kawabe J, Higashiyama S, et al. Heterogeneous liver uptake of Tc-99m-GSA as quantified through SPECT/CT helps to evaluate the degree of liver fibrosis: A retrospective observational study. *Medicine (Baltimore)*. 2018; 97(31): e11765, doi: [10.1097/MD.00000000000011765](#), indexed in Pubmed: [30075603](#).